

A slotted lotus shaped microstrip antenna based an EBG structure

Taha A. Elwi

Communication Department, Al-Mammon University College, Baghdad, IRAQ

Abstract: The objective of this paper is to study intensively the design of a printed slotted patch based lotus shape structure mounted on a dielectric substrate backed with an electromagnetic band Gap (EBG) layer for wideband applications. The dielectric substrate is made of a Roger RT/duroid®5880 layer. An EBG layer is introduced on the back profile of the substrate to provide a high gain bandwidth product over wide frequency bands. The antenna is fed with a novel coplanar waveguide (CPW) structure of a flared geometry; therefore, the ground plane is mounted on the same substrate surface with the patch structure. A conductive trace is introduced at the substrate back from the bottom connected to the CPW through two shoring plates to remove the effects of the EBG layer on the feed structure. The EBG performance and the antenna design methodology are discussed using analytical analyses and numerical parametric studies, respectively. The numerical simulation is conducted using CST MWS Finally; the optimal antenna design is fabricated and measured for validation to be compared to the simulated results.

Keywords: wideband antennas; EBG; CPW; slots

1. Introduction

Recently, a high research impact has been applied on introducing EBG structures to enhance the performance of the microstrip antennas^[1-15]. EBG structures, as a metamaterial, are periodic-like layers of extraordinary surface wave suppression properties with unique features which cannot be found in nature^[1]. Based on their exhibited electromagnetic properties, EBG structures were classified as: near zero refractive index materials^[2], soft and hard surfaces^[3], high-impedance surfaces^[4], and artificial magnetic conductors^[5]. It is worth to mention that some of these structures have several relative electromagnetic properties^[6]. Due to the unique features of the EBG structures, it can be considered as a special type of metamaterials^[4-5] and^[9]; where, their interaction with electromagnetic waves exhibit frequency stop bands, passbands, and band gaps. The concept of EBG structures were originated from the optical domain in 1987^[10] as the terminology of photonic band gap.

Since EBG structures are periodic layers of dielectric or metallic elements arranged as in 1D, 2D, or 3D manners, they provide multiple band gaps based on the unit cell periodicity and the individual unit cell resonance as well^[11]. The EBG performance is highly affected by the macroscopic and microscopic resonances of a periodic structure^[12-13]. Therefore, the macroscopic resonance, Bragg resonance, is governed by the periodicity; while, the lattice resonance controls the microscopic resonance, the unit cell characteristics, to be called the Mie resonance^[8]. Furthermore, the coinciding of the two resonances leads to maximize the structure band gap width. Based on the structure properties and the wave polarization, one of the stop bands dominate over the other bands^[4]. In which, at the stop band, the structure reflects back all incident waves, while at other bands acts as a transparent medium.

According to the literature survey, the EBG structures are classified based on their application domains as in the filter designs, gratings, frequency selective surfaces (FSS)^[14], photonic crystals^[15] and photonic band gaps (PBG)^[11].

Copyright © 2018 Taha A. Elwi.

doi: 10.18063/wct.v2i1.451

This is an open-access article distributed under the terms of the Creative Commons Attribution Unported License

(<http://creativecommons.org/licenses/by-nc/4.0/>), which permits unrestricted use, distribution, and reproduction in any medium, provided the original work is properly cited.

Moreover, the EBG structures are defined as artificial periodic or sometimes non-periodic objects to prevent and/ or assist the incident wave propagation. Besides that, the EBG structures possess high impedance properties such as artificial magnetic conductors. For example, mushroom-like EBG structures exhibits high surface impedances in both TE and TM modes. In which, illuminating the EBG surface creates an in-phase reflection coefficient. Moreover, soft and hard surfaces operate as EBG structures where are identified as frequency wave number planes^[4]. Therefore, such interesting features led to a novel wide range of applications in the antenna engineering researches and industries.

2. Antenna Design and Discussions

The most fundamental challenges to be overcome in the proposed antenna design are the antenna size reduction in flat profile, frequency allocation must be subjected according to the FCC recommendations, high gain enough for medium and long communication distances to be over 2 dB, and $|S_{11}|$ should be less than -10 dB over a wide range of frequencies.

In this section, the performance of the proposed EBG structure in both analytical and numerical aspects is introduced firstly. Whereas, the electromagnetic properties of the proposed EBG structure can be investigated through evaluating the propagation constant, reflection phase and dispersion characteristics of a single unit cell structure. However, in order to realize the enhancements in the introduced microstrip antenna, the author postpone introducing the design methodology for overall structure after EBG structures analysis.

Next, the microstrip patch geometry is derived from a triangular shape. The operation mechanism of each design parameter is optimized in order to determine its initial value. The aim of the proposed design methodology is to maximize the antenna bandwidth in which $|S_{11}| < -10$. The antenna substrate is considered a Roger RT/duroid[®]5880 layer of 0.5mm thickness (h) and $\epsilon_r=2.2$ with $\tan\delta=0.0009$. The overall antenna dimensions are 32mm×28mm in length and width, respectively. In the proposed design, a 50Ω feed line is connected to the patch and printed on the substrate. Therefore, the antenna design methodology is presented by the flow chart that is seen in **Figure 1**.

EBG construction and performance

The proposed EBG structures are printed on the back panel of the substrate for two purposes: Suppresses the surface waves on the substrate and reduces the interference of the surface current on the ground plane edges ^[16]. The EBG layer is constructed of 6×7 array of square metal pads, to create 5×6 slots, mounted on a rectangular area of 24mm×28mm as seen in **Figure 2(a)**. The dimensions of the proposed unit cell, see **Figure 2(b)**, are 4mm×4mm. The EBG structure is based on conductive square pads (p) of 3.6mm×3.6mm size spaced with a gap (g) 0.4 mm mounted on the substrate.

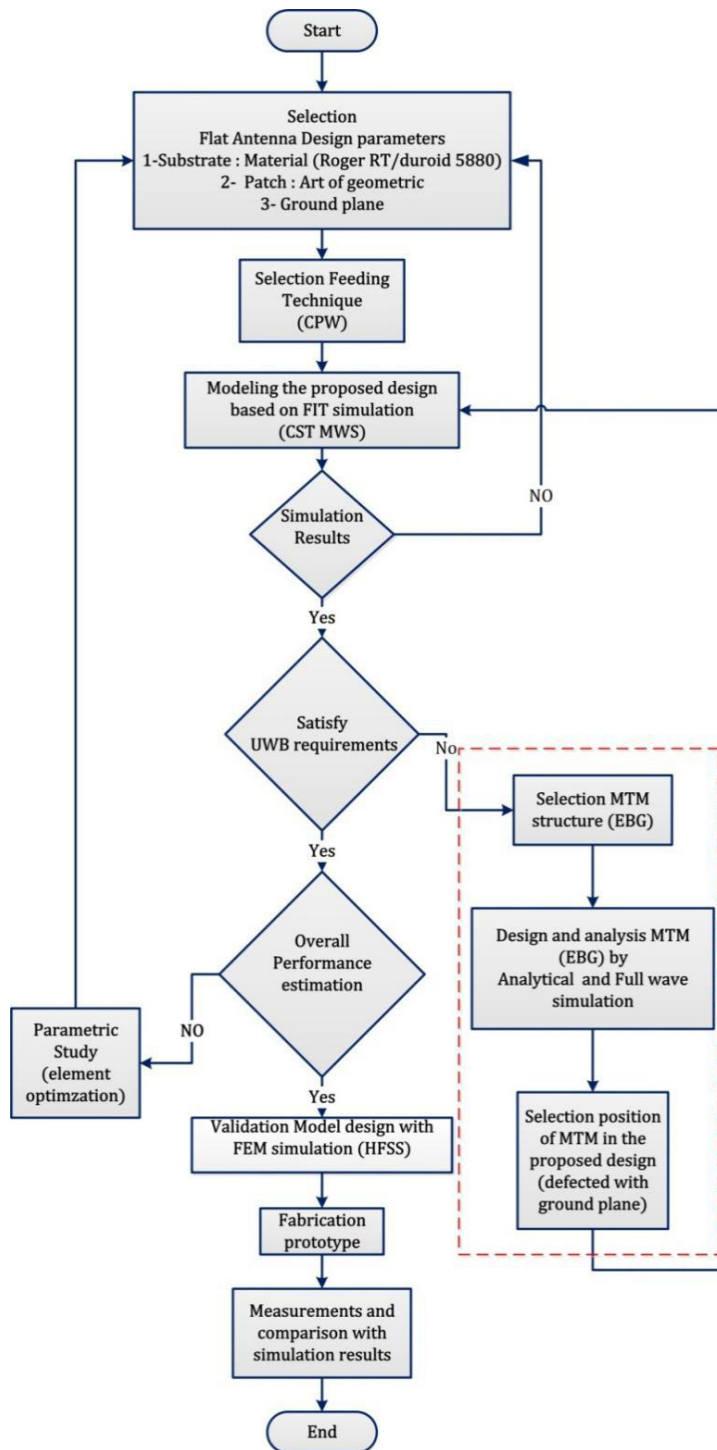


Figure 1; Flow chart of the proposed antenna design methodology.

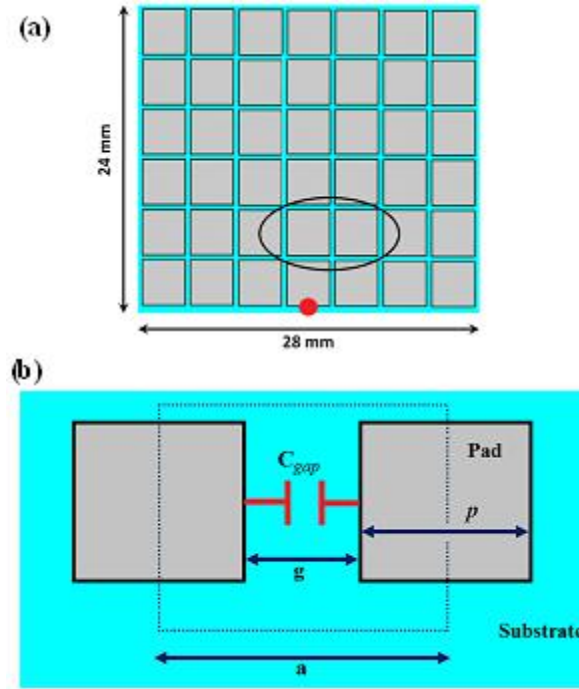


Figure 2; The proposed EBG structure: (a) the EBG array based on 6×7 unit cells. and (b) the capacitor equivalent of the unit cell slot. Note: The red point represents the excitation location.

Such array creates a capacitive gap (C_{gap}) between neighboring cells which can be calculated using the following formula^[16].

$$C_{gap} = \frac{p\epsilon_0(1 + \epsilon_r)}{\pi} \cosh^{-1} \left(\frac{p + g}{\alpha} \right) \quad (1)$$

The proposed EBG structures exhibit a capacitive behavior, so works as high pass filter that allows passing the high frequencies and prevent the lower bands. On the other hand, each unit cell can be considered unbalanced circuit because the inductive absence where the influence of the capacitive reactance on the EBG width is higher than its length for the surface current.

$$X_c = \frac{1}{2\pi f C_{gap}} \quad (2)$$

One of the main factors which control the proposed EBG performance is the number of slots ($m \times n$) in their array. For this analysis, the number of slots along the length (m) is considered 5, and the number of slots along the width (n) is considered 6. However, it is worth to mention that the EBG slots repetition on the width influence has been selected depending on the size of proposed EBG structure and the maximum size of the antenna and the fabrication limitation. So, the capacitive reactance between the unit cells on the width has higher suppression for surface currents.

For an additional validation, the dispersion diagram based on CST MWS and reflection phase based on Agilent ADS are realized. The Eigen mode simulation of the CST MWS formulations is invoked to localize the band-gap, the natural resonances and the dispersion properties that are exhibited by the proposed EBG unit cell. The dispersion characteristics of the TE and TM modes can be performed at the First Brillion Zone (FBZ)^[17] in the crystal lattice (Γ, χ, M) vertex. This is by considering a triangle of two equidistant sides (Γ to X and X to M), while, the other longer side is (M to Γ). Each side can be described by a dispersion characteristics graph that can be merged in one continues dispersion diagram.

From the resulted dispersion diagram, see **Figure 3**, the horizontal axis represents phase differences along FBZ boundaries. However, it is seen in the frequency range of interest that the structure supports a fundamental TM mode which electric filed is mostly longitudinal to the direction of the propagation, followed by TE mode which is predominantly transverse to the direction of propagation. Consequently, any propagation can be considered prohibited in TM mode under 8 GHz while in TE mode under 12 GHz.

The propagation constant (γ) for the proposed unit cell can be expressed with the absence of the inductance component as:

$$\gamma = \sqrt{R(G + j\omega C_{\text{gap}})} \quad (3)$$

Such γ involves only the conductor and the dielectric losses in R and G, respectively, are dispersive values in dB and given in [21] as:

$$R \approx \frac{8.686 \sqrt{\pi t \mu / \sigma}}{2\pi \epsilon_0 h} \times \left[1 - \left(\frac{p}{4h} \right)^2 \right] \times \left[1 + \frac{p}{p'} + \frac{p}{h} \left(\ln \frac{2h}{p'} - \frac{t}{h} \right) \right] \quad (4)$$

$$G \approx 8.68\pi \frac{\epsilon_r - 1}{\epsilon_r} \times \frac{\tan \delta}{\lambda} \quad (5)$$

where μ is permeability of the conductor, σ is conductivity, t conductor thickness, and λ_g is the guide wavelength.

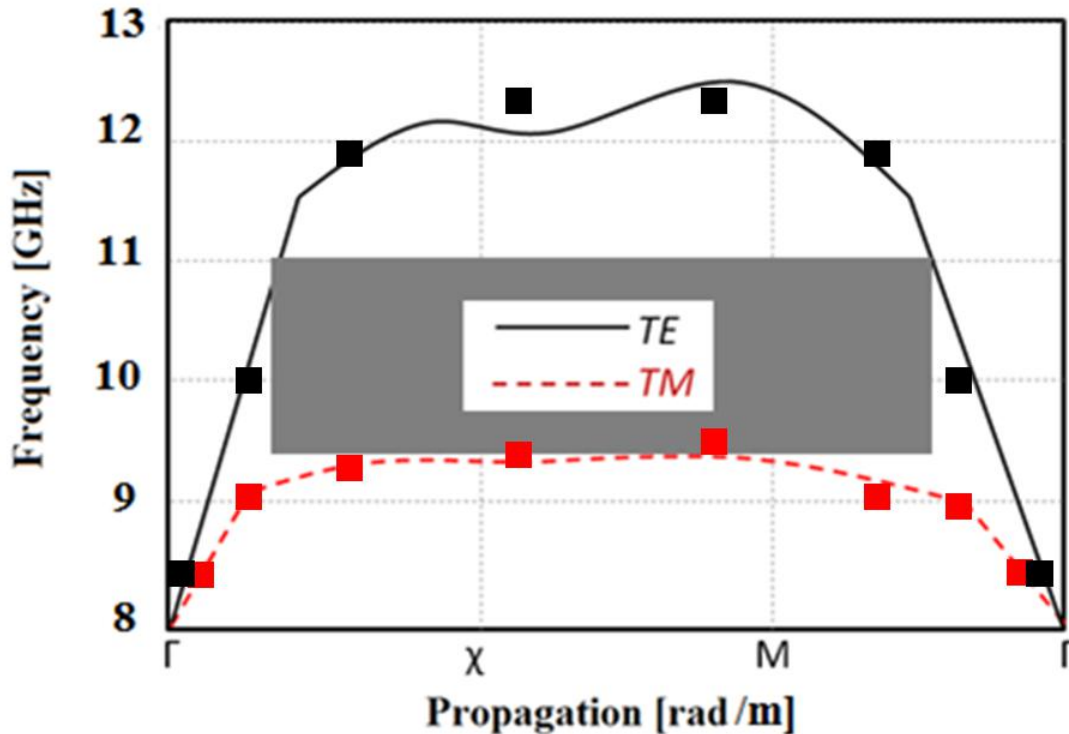


Figure 3; Dispersion properties of the proposed EBG unit cell, where, the lines for the CST MWS simulation results and the square symbols are for the analytical results.

ADS simulation is carried out for characterizing the reflection characteristics in terms of phase in order to validate the effects of adding the EBG pads on the antenna performance. From **Figure 4**, the simulation is evaluated based on the transmission line circuit via creation of several concatenated TL and layouts embedded as sub networks within a single design. Finally, the analytical expressions based on the derived analysis in^[18] are compared to the results of CST and ADS simulations.

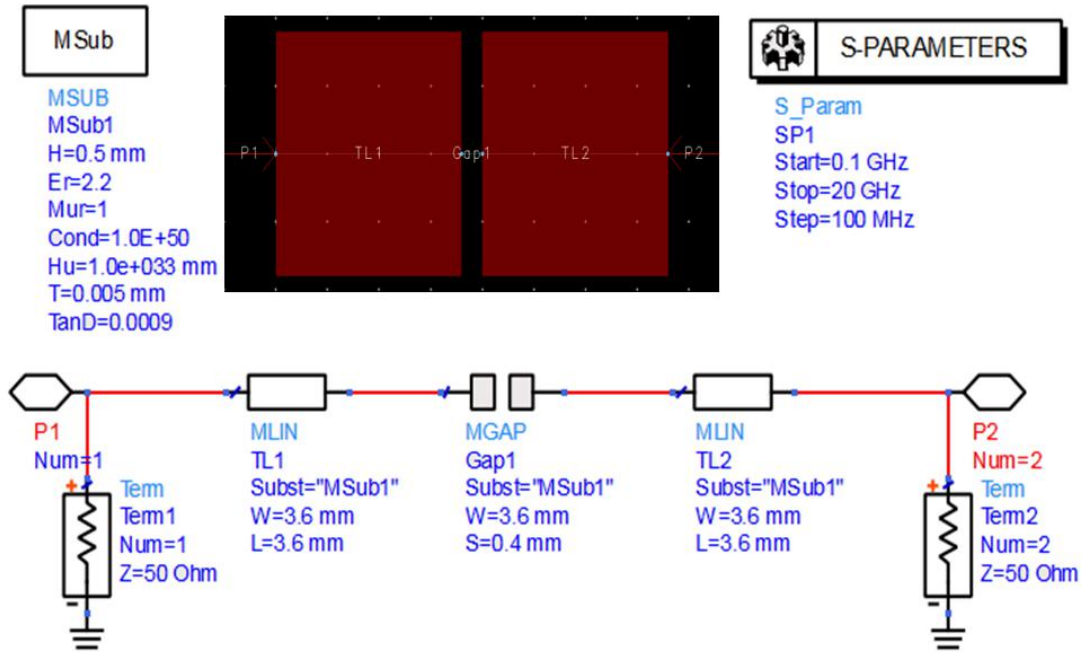


Figure 4; The modeling of the EBG unit cell in the ADS schematic window.

It is found that the unit cell shows reflection phase behavior between the 8 GHz and 12 GHz as shown in **Figure 5(a)**. Nevertheless, the electromagnetic properties including ϵ_r and μ_r for the proposed unit cell are evaluated and presented in **Figure 5(b)** with and without substrate. It is found that the introduction of the substrate layer has a significant effect on the retrieved ϵ_r and μ_r due to the change of the guided wave length^[10].

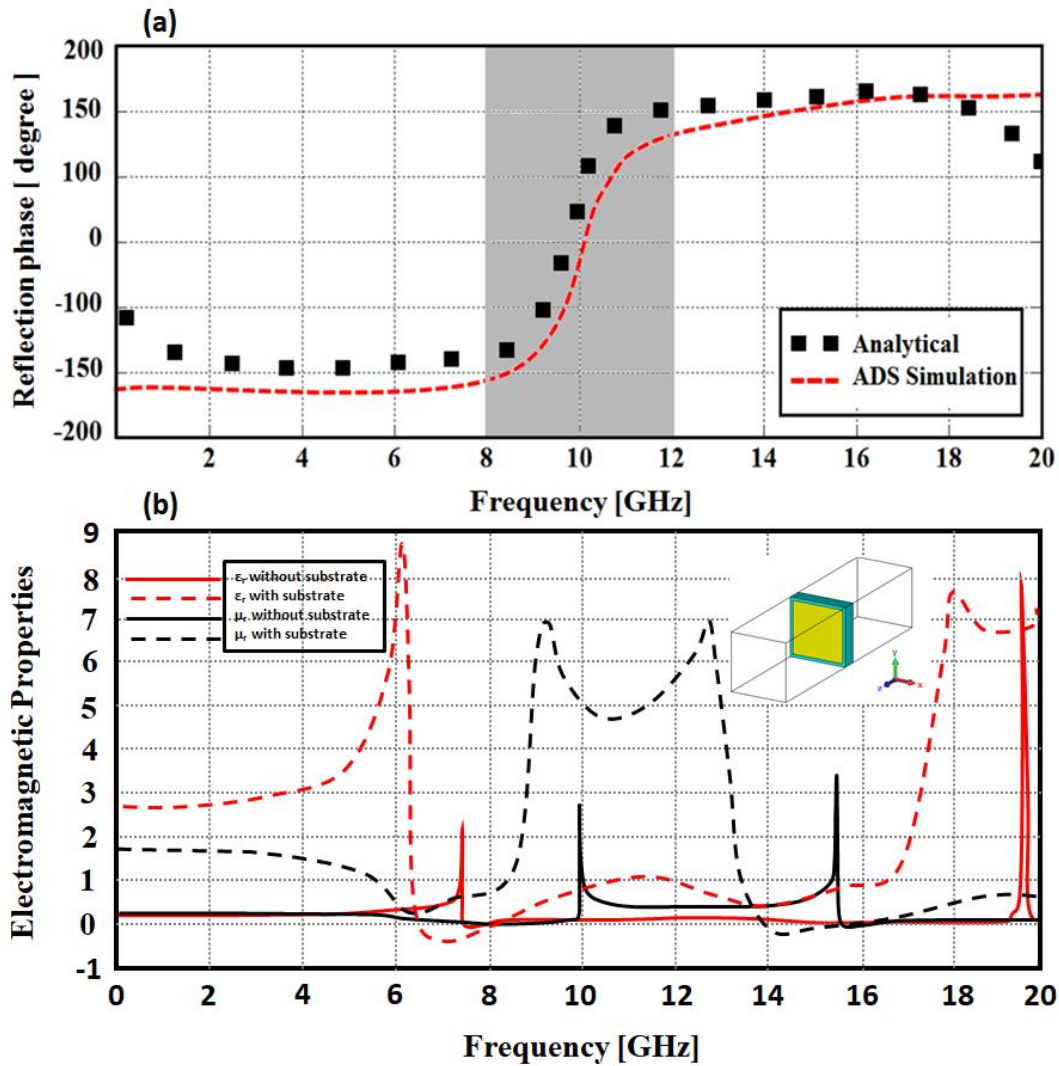


Figure 5; The unit cell characteristics including; (a) Reflection phase and (b) Relative electromagnetic properties.

Antenna design methodology

The antenna design methodology, with the parameters depicted in this section, has been modeled step by step. The antenna exhibits a wideband response with an impedance bandwidth of $|S_{11}| < -10\text{dB}$. Therefore, the antenna design derivation steps are presented as:

The First design modeling (Antenna 1)

Figure 6 shows the geometry of the microstrip antenna (Antenna 1) based on a triangular geometry. The antenna design is started from an equilateral triangular patch backed with a full ground plane of dimensions are depicted in Table 1. The S_{11} spectrum is evaluated by CST MWS as seen in **Figure 7**. It is found that such antenna design provides narrow bandwidths around multiple frequency bands.

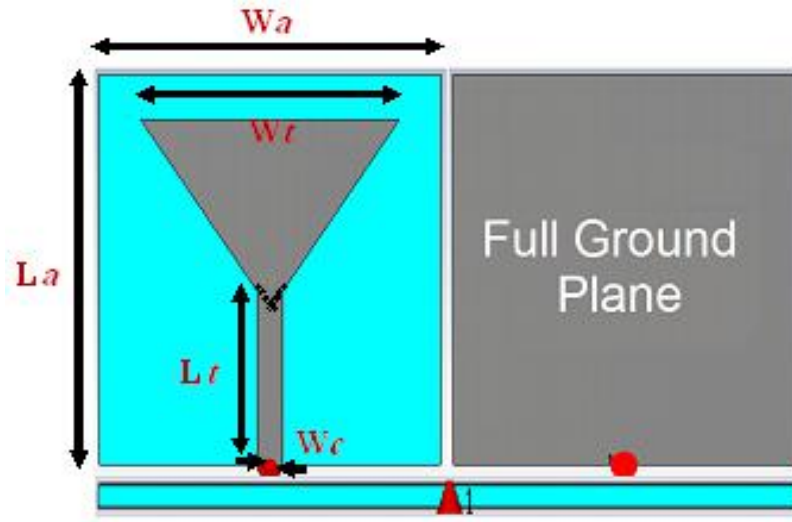


Figure 6; The proposed model antenna 1.

Description	Parameter	Value (mm)
Substrate width	W_a	28
Substrate length	L_a	32
Patch width	W_t	21
Feed-line length	L_t	12.5
Feed-line width	W_c	1.2

Table 1. Initial dimensions for the antenna 1.

The S_{11} spectra of the Antenna 1, shown in **Figure 8**, are carried out of different patch Widths (W_t). It is found that W_t variation has an effect on the antenna bandwidth as well as the center frequency. While, **Figure 9** shows the S_{11} spectra of the Antenna 1 after varying the length of the feed line (L_t). It is observed that the L_t variation has insignificant effects on the center frequency.

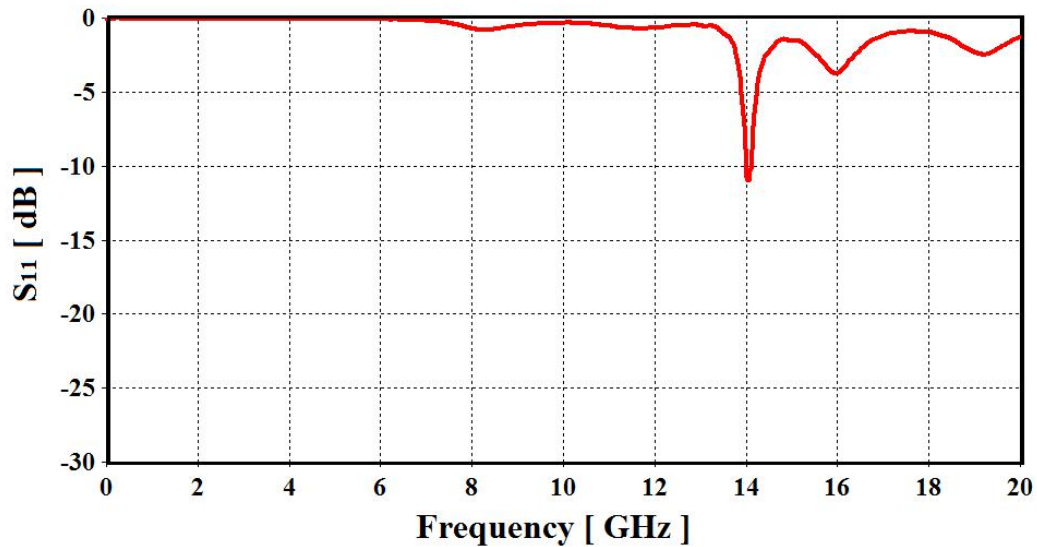


Figure 7: S_{11} spectrum for the Antenna 1.

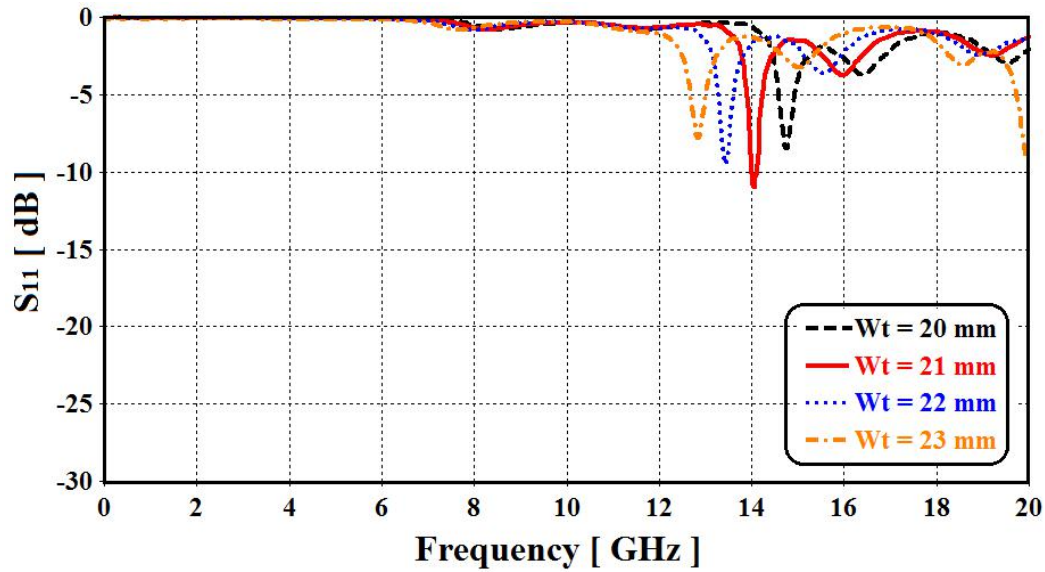


Figure 8; The S_{11} spectra variation with respect to W_t change.

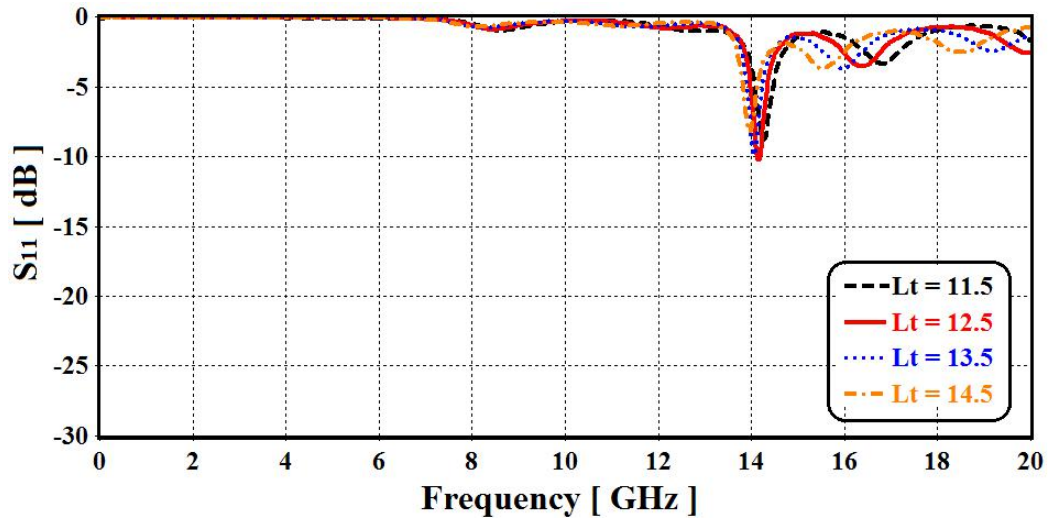


Figure 9; The S_{11} spectra variation with respect to L_t changes.

The S_{11} changes with different feed line widths (W_c) are shown in Figure 10. It is shown the matching can be improved by increasing W_c .

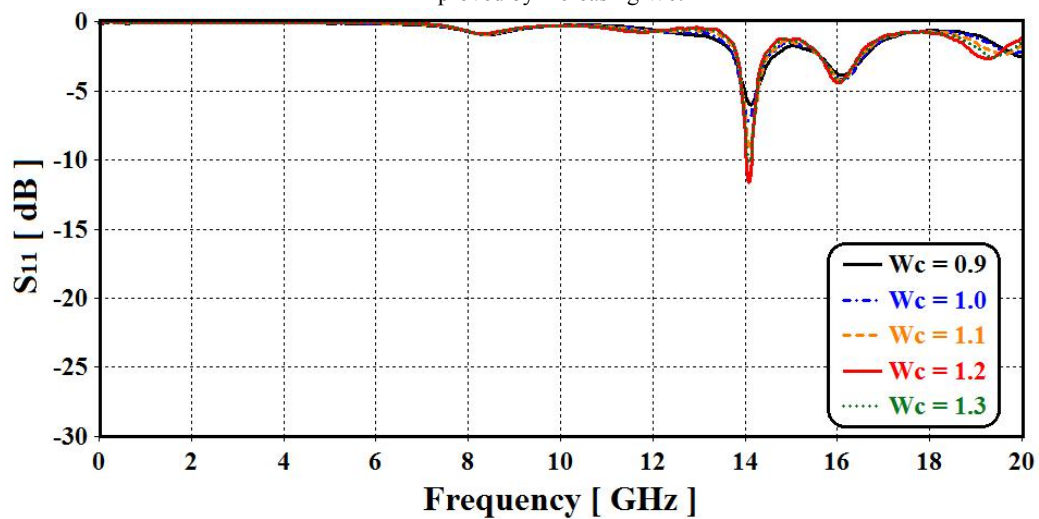


Figure 10; The S_{11} spectra variation with respect to W_c changes.

The second design modeling (Antenna 2)

In this section, the ground plane with antenna 1 is changed to a partial conductive geometry as seen in **Figure 11** to be called Antenna 2. By optimizing the ground plane dimensions as shown in Table 5, a significant enhancement is achieved in the bandwidth; however, with poor matching. The partial ground plane removal reduces the back-lobe radiation of the proposed antenna by suppressing the surface wave diffraction from the edges of the ground plane^[12]. **Figure 12** shows the S_{11} of the Antenna 2.

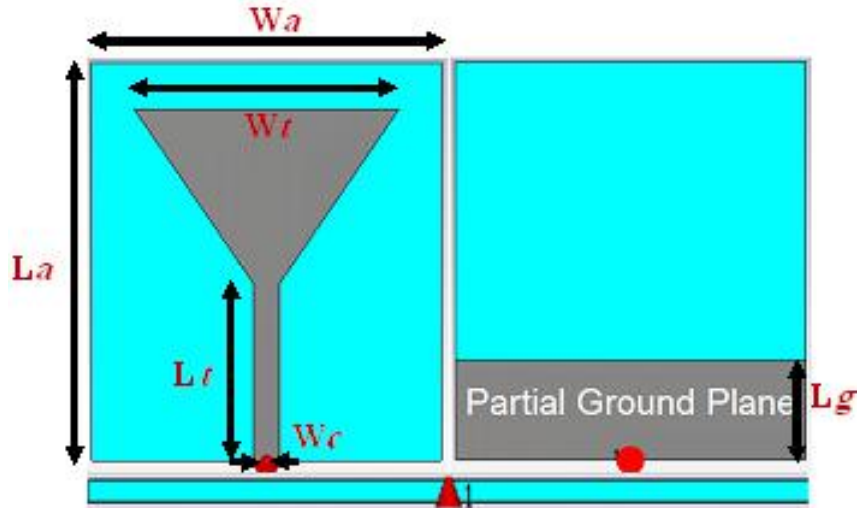


Figure 11; The proposed model antenna 2.

Description	Parameter	Value (mm)
Substrate width	W_a	28
Substrate length	L_a	32
Patch width	W_t	21
Feed-line length	L_t	12.5
Feed-line width	W_c	1.2
Ground plane length	L_g	8

Table 5; Initial dimensions for the antenna 2.

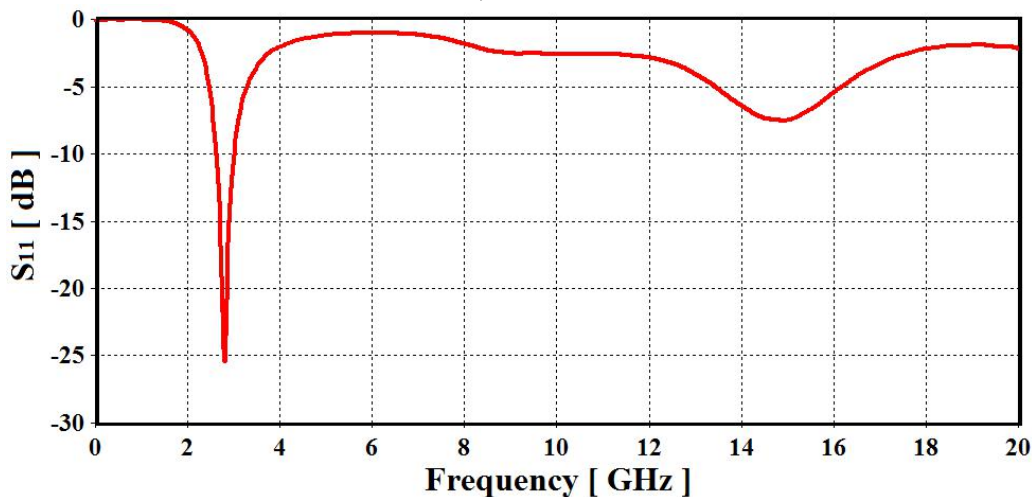


Figure 12; S_{11}

spectrum for the Antenna 2.

A sweep of the parameter (L_g) has been taken, where **Figure 13** shows samples of the S_{11} spectra of L_g sweep. It is clearly shown that the variation of L_g has a little shift in the center frequency.

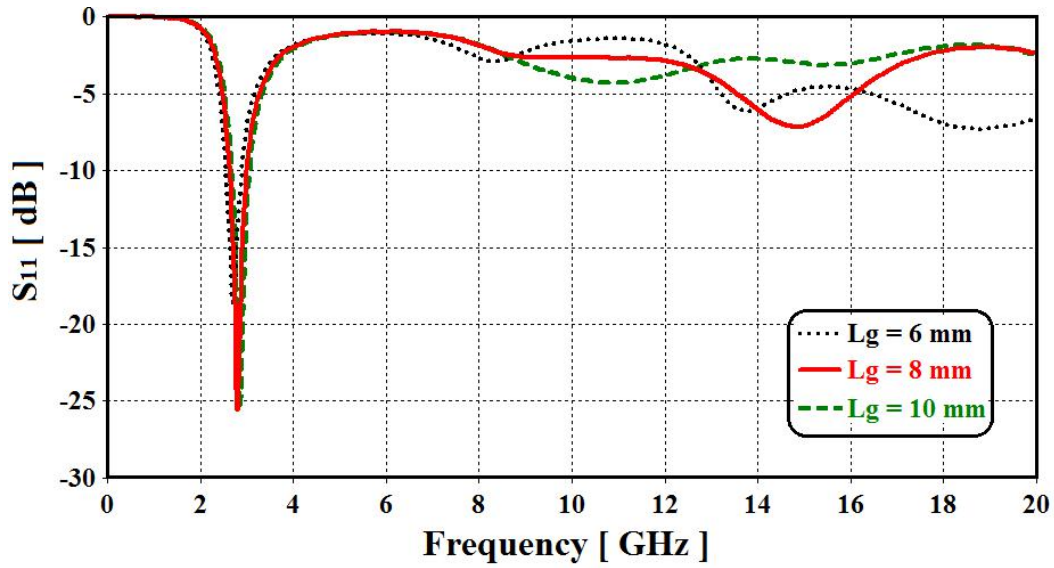


Figure 13; The S_{11} spectra variation with respect to L_g change.

The second design modeling (Antenna 3)

The Antenna 2 is developed to the model in Antenna 3 as seen in **Figure 14** by using a coplanar transmission line with flared ground planes from to connect the SMA port to the patch continuously. Such novel feeding desing is adopted to maximize the matching between the input impedance of the patch and the SMA over a wide range of frequencies. Nevertheless, the flared ground planes act as matching circuits as well as reflectors in which the electromagnetic radiation may towards to the end-fire direction. The geometrical dimensions of the antenna and the relative S_{11} spectra are shown in Table 7 and **Figure 15**, respectively.

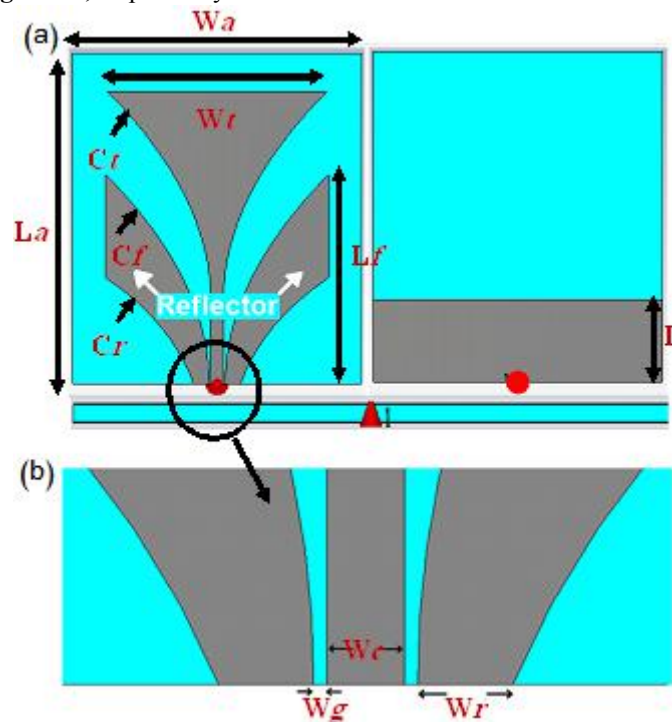


Figure 14; The proposed model antenna 3 (a) the flared geometry of the reflectors and (b) the coplanar transmission line dimension.

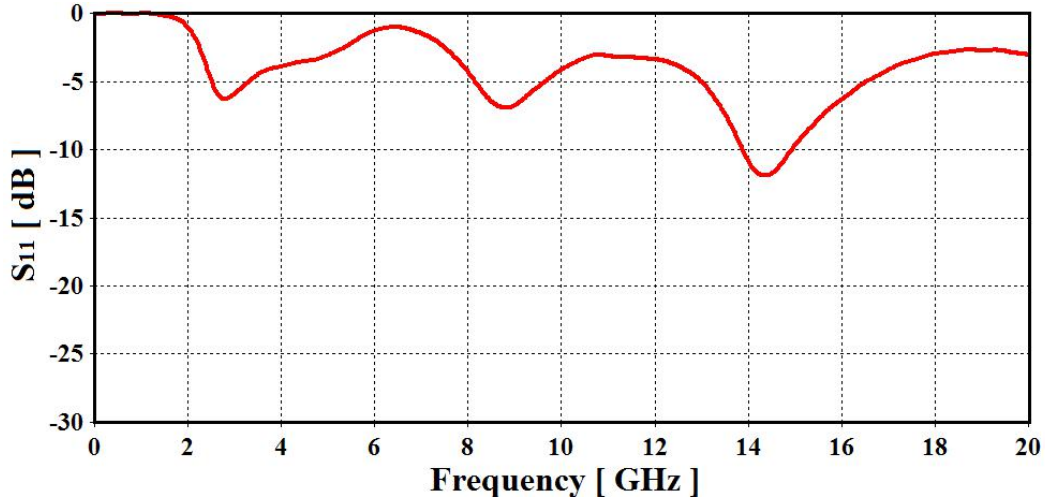


Figure 15; S_{11} spectrum for the Antenna 3.

The novel CPW structure is modified from a traditional CPW based on introducing the flair geometry based on a binomial exponential curve that is calculated according to the following equations after considering the substrate height and $\epsilon_{eff}^{[1]}$.

$$Z_{n+1} = Z_n \exp \left[2^{-N} \ln \left(\frac{R_l}{r} \right) C_n^N \right] \quad (6)$$

$$C_n^N = \frac{N!}{(N-n)!n!} \quad (7)$$

$$Z_{n+1} = \frac{120\pi}{\sqrt{\epsilon_{eff}} [W/h + 1.393 + 0.667 \ln (W/h + 1.444)]} \quad (8)$$

$$\epsilon_{eff} = \frac{\epsilon_r + 1}{2} + \frac{\epsilon_r - 1}{2} \frac{1}{\sqrt{1 + 12h/W}} \quad (9)$$

where, Z_{n+1} is the characteristics impedance, ϵ_{eff} is the effective dielectric constant, and h is the substrate height, N is the stage number, n is number of stages which it is 200.

Description	Parameter	Value (mm)
Substrate width	Wa	28
Substrate length	La	32
Patch width	Wt	21
Flared length	Ct	$y_1 = 3.18e^{Rx} - 11.56$ $\frac{W_c}{2} \leq x \leq \frac{W_t}{2}$
Reflector length (Top side)	Cf	$y_2 = 3.06e^{Rx} - 19.56$ $\frac{W_c}{2} + W_g \leq x \leq \frac{W_t}{2}$
Reflector length (down side)	Cr	$y_3 = 1.64e^{Rx} - 18.52$ $\frac{W_c}{2} + W_g + W_r \leq x \leq \frac{W_t}{2}$
Reflector length	Lf	20
Feed-line width	Wc	1.2
Ground plane length	Lg	8
Gap width between Reflector and feed line	Wg	0.2
Reflector width-down	Wr	1.45

Table 7. Initial dimensions for the antenna 3.

This section represents the effects of changing the reflector length (L_f) on the bandwidth. From **Figure 16**, it can be seen that increasing L_f restricts the bandwidth.

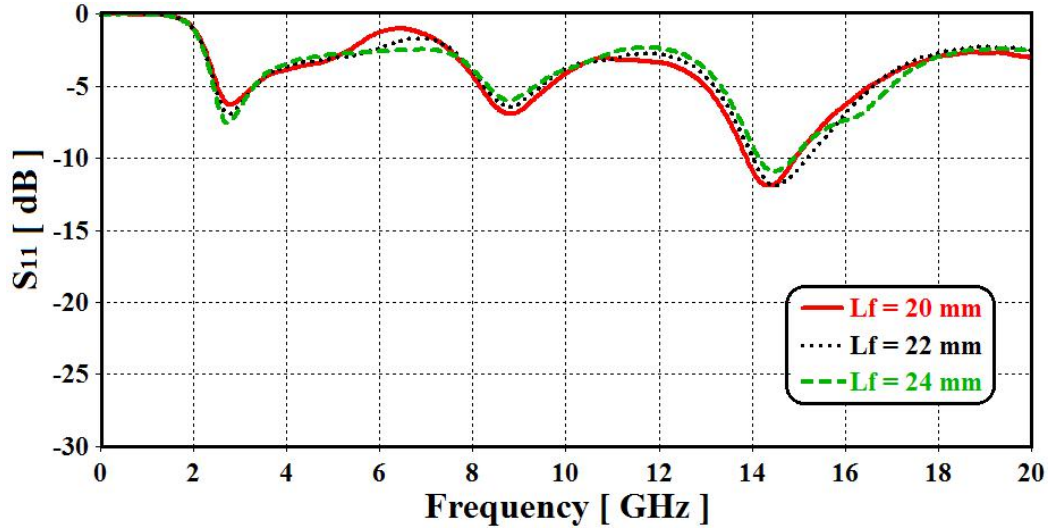


Figure 16; The S_{11} spectra variation with respect to L_f change.

The best separation distance between the reflectors and the transmission line can be localized to maximize the matching. The effects of separation distance on the S_{11} spectra are monitored by changing it as 0.05 mm, 0.1 mm, and 0.15 mm as seen in **Figure 17**. It is found that the coupling gap exhibits a significant effect on the antenna bandwidth.

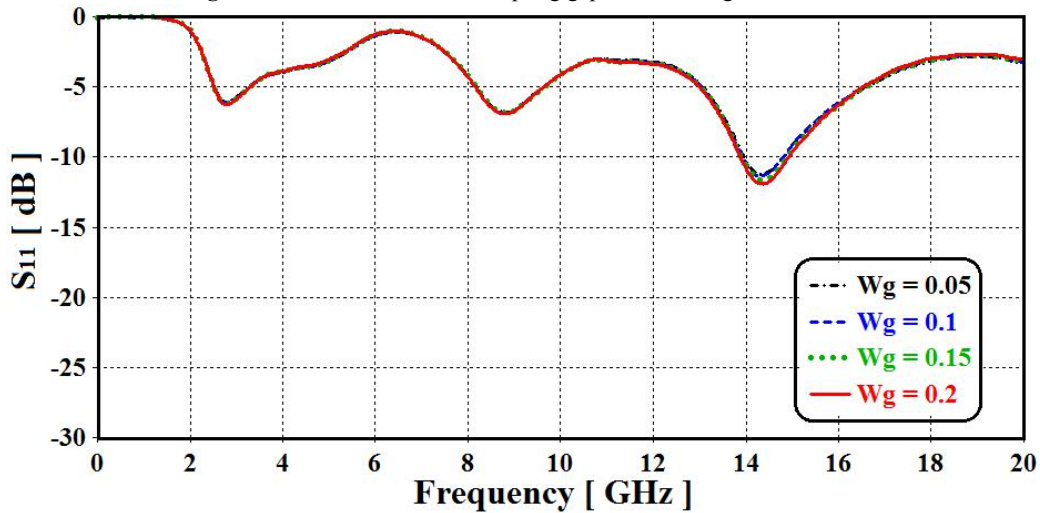


Figure 17; The S_{11} spectra variation with respect to W_g change.

The second design modeling (Antenna 4)

A further modification is considered in this design as presented in Antenna 4 by including triangular slots on the patch to create new resonance modes by increasing surface current paths on the patch. Then, the surface electrical area of the patch within the same physical area is increased. **Figure 18** and Table 8 show the antenna configuration and design parameters, respectively. In addition, the internal areas of the coplanar transmission line reflectors are etched to improve the matching impedance of the antenna as shown in **Figure 19**. Furthermore, removing the internal area of the coplanar transmission line reflectors insures the avoidance of any possibility of the radiation coupling effects due to the current motion on the conductor surface^[13] that may led to side radiation lobes.

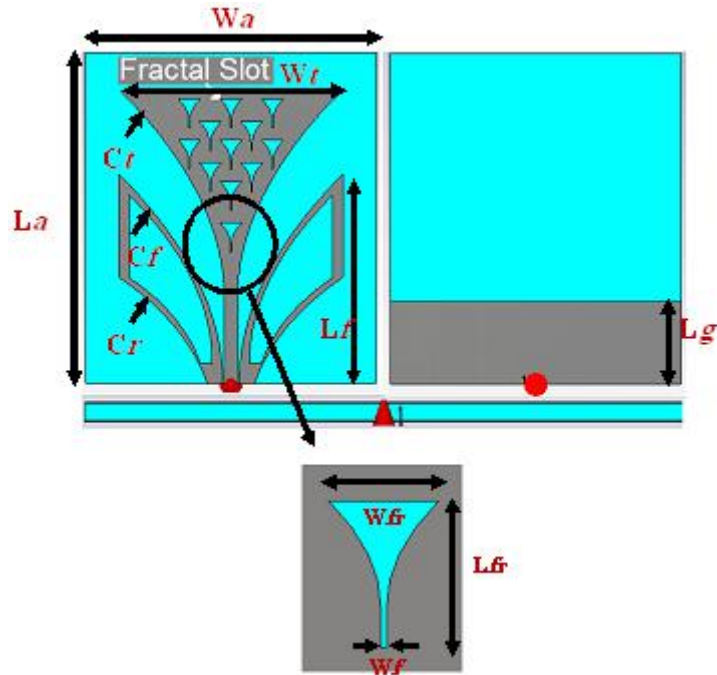


Figure 18; The proposed antenna 4 with triangular slots.

Description	Parameter	Value (mm)
Substrate width	Wa	28
Substrate length	La	32
Patch width	Wt	21
Flared length	Ct	$y_1 = 3.18e^{Rx} - 11.56$ $\frac{W_c}{2} \leq x \leq \frac{W_t}{2}$
Reflector length (Top side)	Cf	$y_2 = 3.06e^{Rx} - 19.56$ $\frac{W_c}{2} + W_g \leq x \leq \frac{W_t}{2}$
Reflector length (down side)	Cr	$y_3 = 1.64e^{Rx} - 18.52$ $\frac{W_c}{2} + W_g + W_r \leq x \leq \frac{W_t}{2}$
Reflector length	Lf	20
Feed-line width	Wc	1.2
Ground plane length	Lg	8
Gap width between Reflector and feed line	Wg	0.2
Reflector width-down	Wr	1.45
Fractal width-top	Wfr	2
Fractal width-down	Wf	0.1
Fractal length	Lfr	2.8

Table 8. Initial dimensions for the antenna 4.

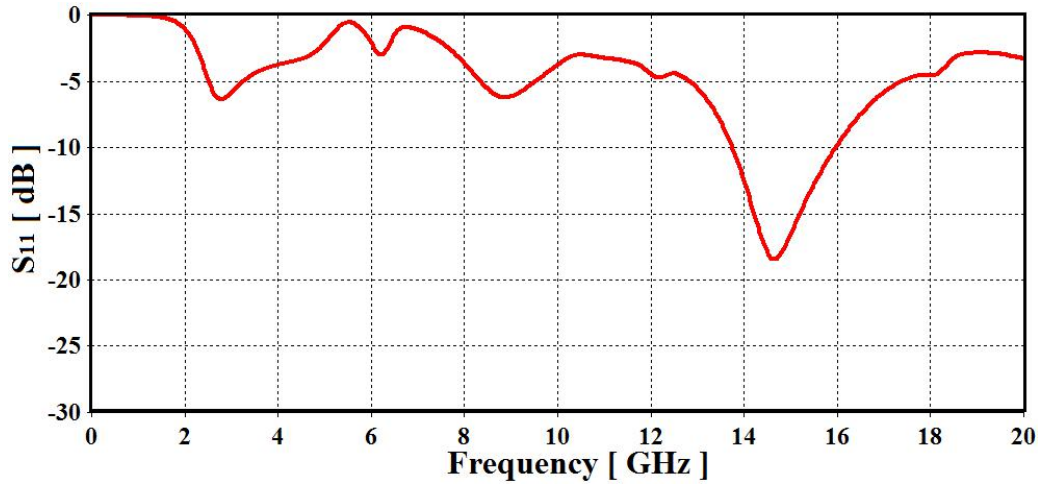


Figure 19; S_{11} spectrum for the Antenna 4.

A sweep of the parameter (W_{fr}) has been taken in to account. **Figure 20** shows samples of the return loss responses of the sweep of the fractal width W_{fr} . It is obvious that the variation of the width has insignificant effects on the center frequency position only.

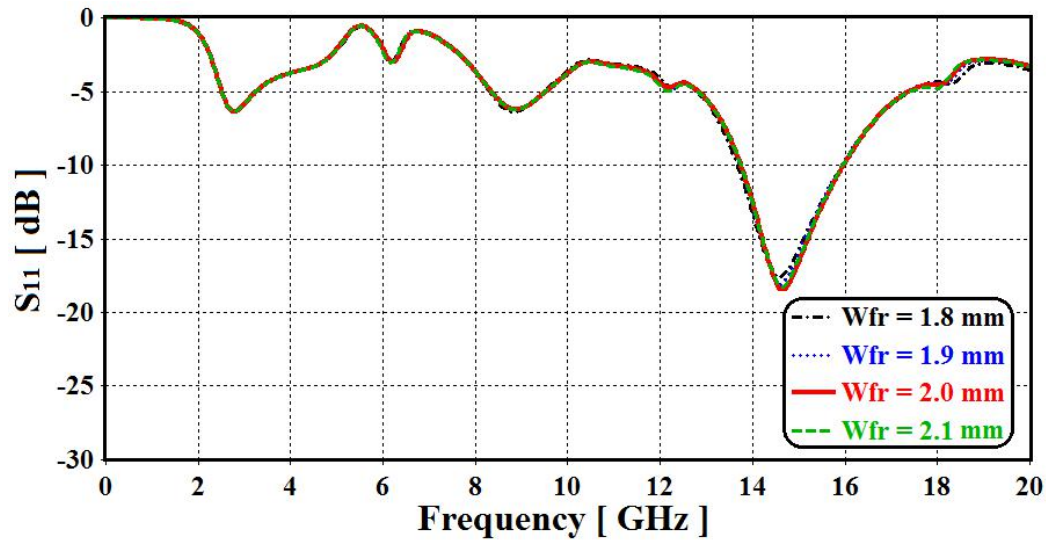


Figure 20; The S_{11} spectra variation with respect to W_{fr} change.

Figure 21 shows the S_{11} spectra of the modeled antenna after changing the length of the slot (L_{fr}). It is clearly shown that the variation of L_{fr} value has a little effect on the center frequency.

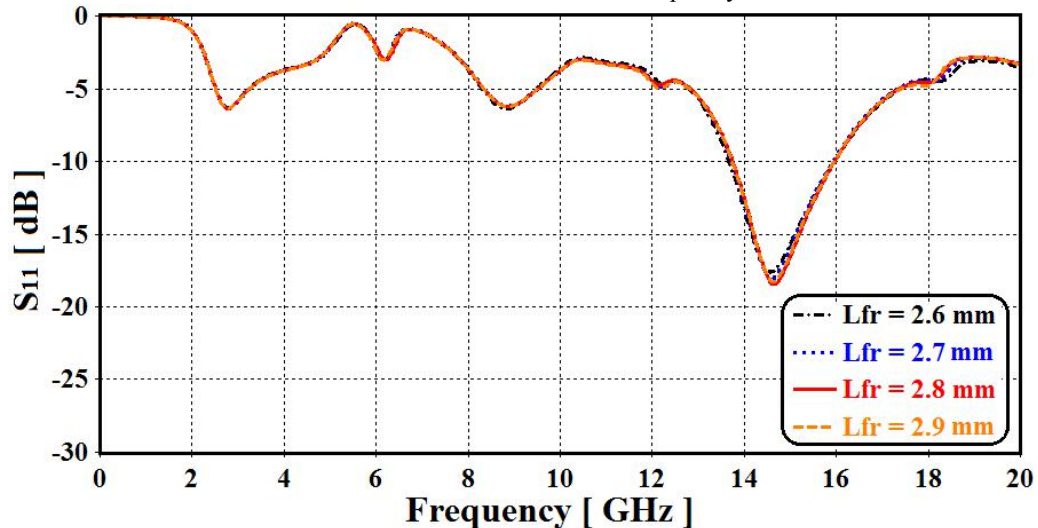


Figure 21; The S_{11} spectra variation with respect to L_{fr} change.

It is worth to mention that the surface current of the antenna with solid reflector is mainly distributed along the edges of the reflector as seen **Figure 22**. Therefore, both reflectors are etched to improve the directivity and reduced the side lobes without extending the antenna dimensions.

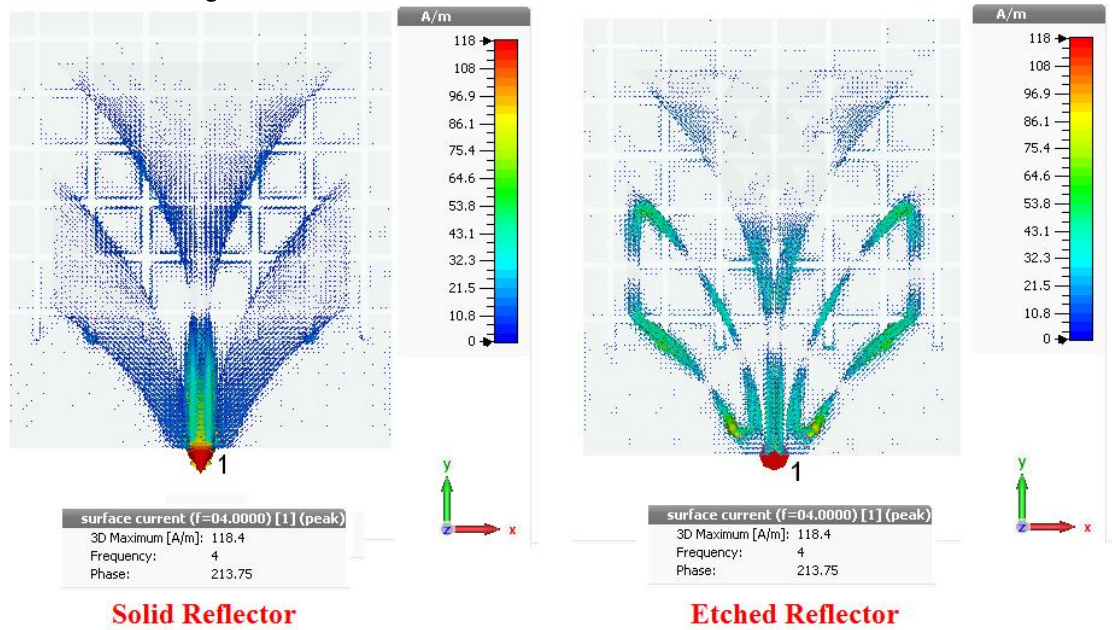


Figure 22; Surface current distribution is presented at 4 GHz as an example of other frequencies.

Design the Reference Antenna with Shorting Plates (Antenna 5)

In this section, the Antenna 4 are modified to Antenna 5 by adding shorting plates to the coplanar waveguide to work as matching circuits as shown in **Figure 23**. The antenna dimensions and the S_{11} spectrum are presented in Table 10 and Figure 24, respectively.

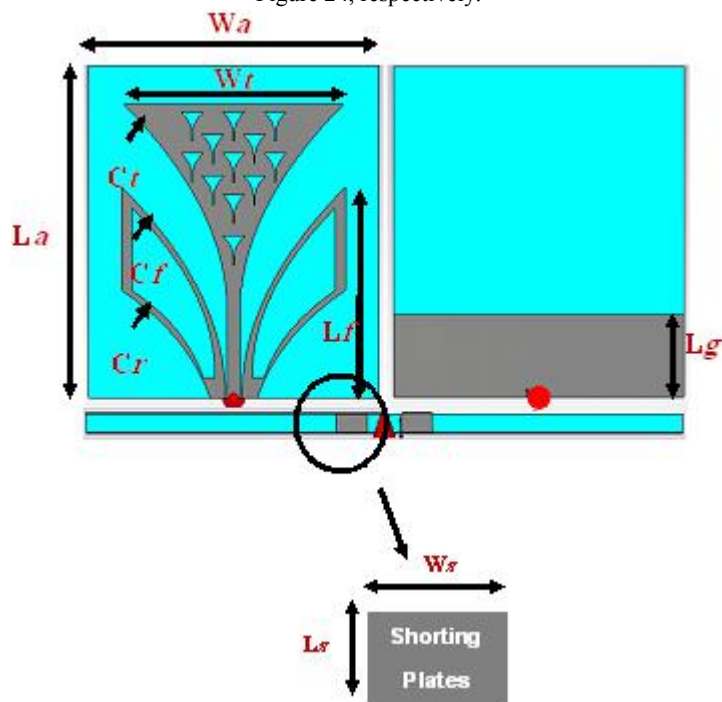


Figure 23;(a) the proposed reference antenna with shorting plates and (b) shorting plate dimensions.

Description	Parameter	Value (mm)
-------------	-----------	------------

Substrate width	Wa	28
Substrate length	La	32
Patch width	Wt	21
Flared length	Ct	$y_1 = 3.18e^{Rx} - 11.56$ $\frac{W_c}{2} \leq x \leq \frac{W_t}{2}$
Reflector length (Top side)	Cf	$y_2 = 3.06e^{Rx} - 19.56$ $\frac{W_c}{2} + W_g \leq x \leq \frac{W_t}{2}$
Reflector length (down side)	Cr	$y_3 = 1.64e^{Rx} - 18.52$ $\frac{W_c}{2} + W_g + W_r \leq x \leq \frac{W_t}{2}$
Reflector length	Lf	20
Feed-line width	Wc	1.2
Ground plane length	Lg	8
Gap width between taper- shaped and feed line	Wg	0.2
Reflector width-down	Wr	1.45
Fractal width-top	Wfr	2
Fractal width-down	Wf	0.1
Fractal length	Lfr	2.8
Shorting plate width	Ws	1.45
Shorting plate length	Ls	0.5

Table 10. Reference antenna with shorting plate dimensions.

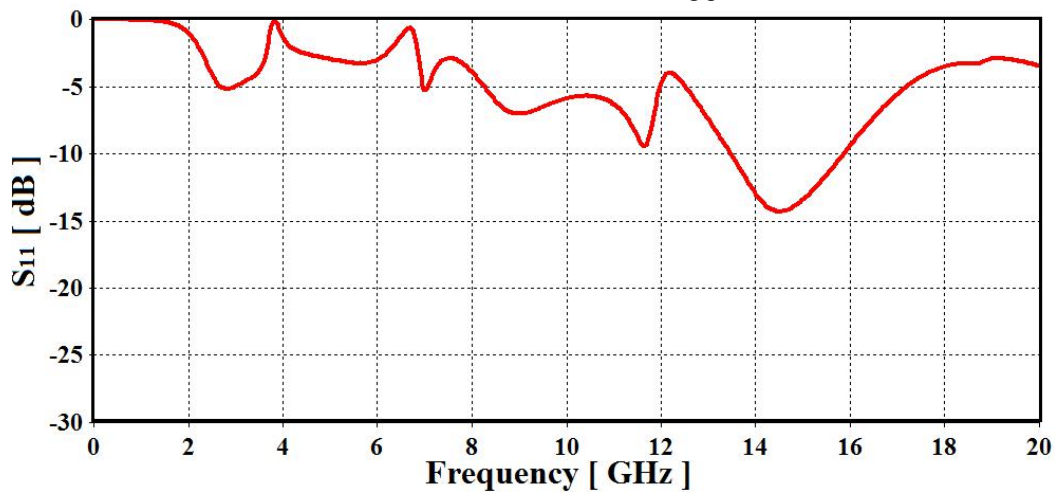


Figure 24; The S_{11} spectra of the Antenna 5.

The return loss responses of the modeled antenna, shown in **Figure 25**, have been carried out for different sizes of the shorting plate width (W_s) as it is shown in Table 11. It is obvious that the variation of the width has insignificant effects on the center frequency position.

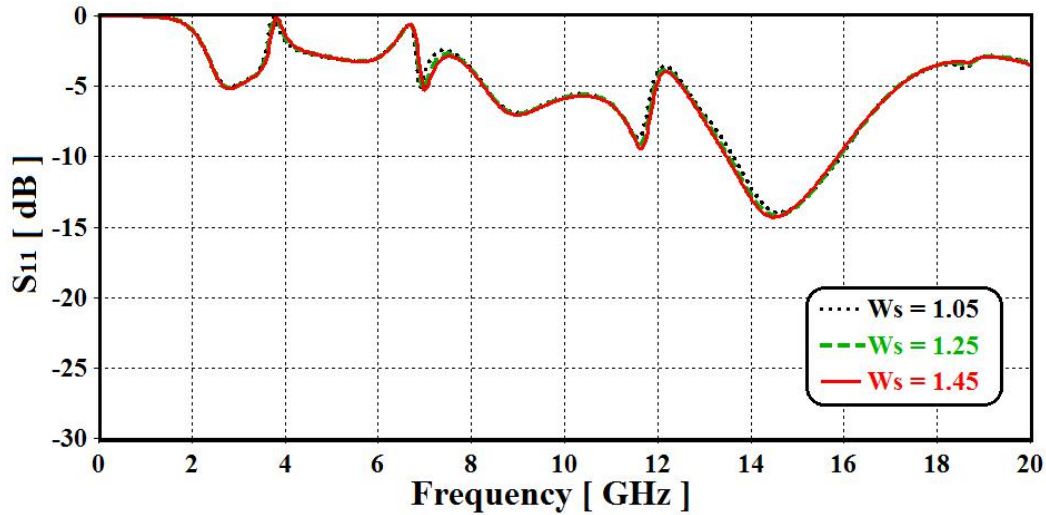


Figure 25; The S_{11} spectra variation with respect to W_s change.

Design the Reference Antenna with EBG Structures (Antenna 6)

Finally, the EBG-defects are introduced, see **Figure 26**, to the partial ground plane of Antenna 5 to improve the antenna matching. Excellent enhancements are found in the antenna directivity, gain and beamwidth due to suppressing the surface waves. These EBG structures on the ground plane are defected as square pads to enhance the tangential component of the electric field and the broadness the antenna radiation toward the end fire. For the proposed antenna design, Antenna 6, all the related parameters are described in Table 11. The S_{11} spectrum is presented in **Figure 27** with excellent enhancements in the bandwidth.

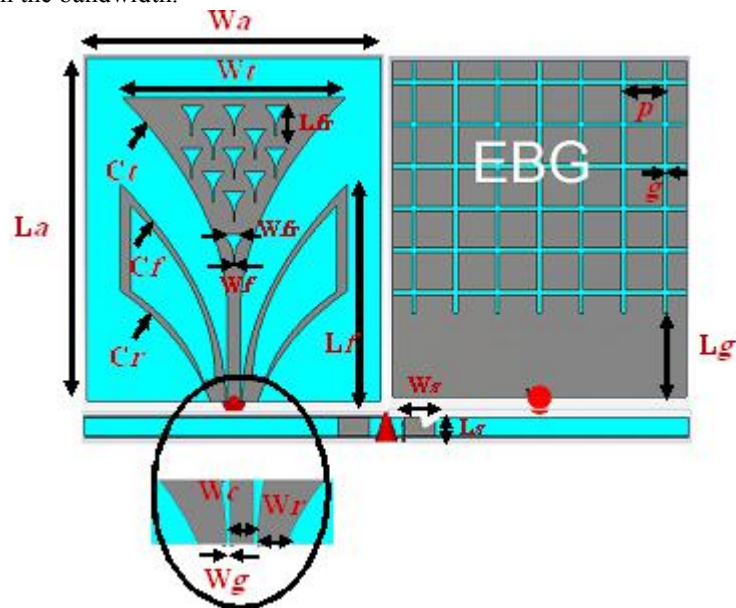


Figure 26; The final proposed wideband antenna with EBG structures.

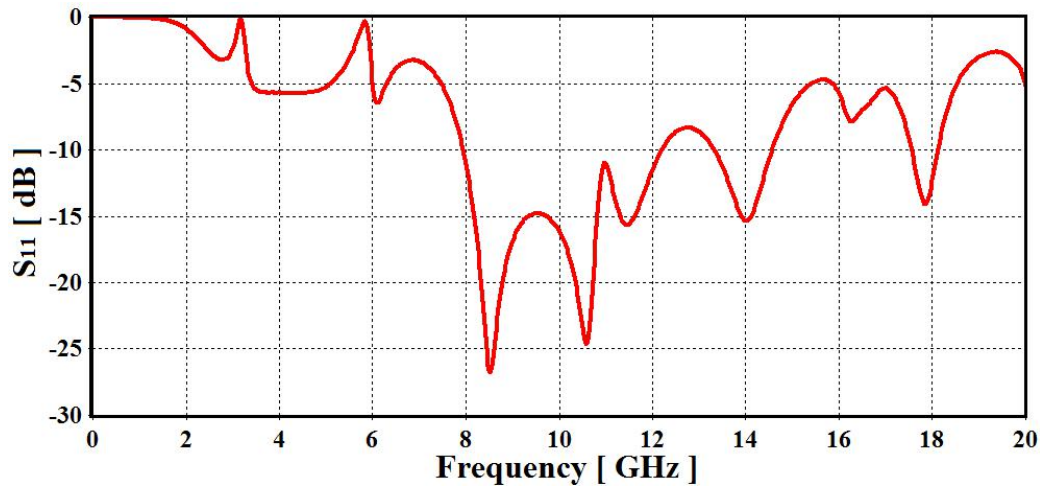


Figure 27; The S_{11} spectrum for the final Antenna 6.

Description	Parameter	Value (mm)
Substrate width	Wa	28
Substrate length	La	32
Patch width	Wt	21
Flared length	Ct	$y_1 = 3.18e^{Rx} - 11.56$ $\frac{W_c}{2} \leq x \leq \frac{W_t}{2}$
Reflector length (Top side)	Cf	$y_2 = 3.06e^{Rx} - 19.56$ $\frac{W_c}{2} + W_g \leq x \leq \frac{W_t}{2}$
Reflector length (down side)	Cr	$y_3 = 1.64e^{Rx} - 18.52$ $\frac{W_c}{2} + W_g + W_r \leq x \leq \frac{W_t}{2}$
Reflector length	Lf	20
Feed-line width	Wc	1.2
Ground plane length	Lg	8
Gap width between taper- shaped and feed line	Wg	0.2
Reflector width-down	Wr	1.45
Fractal width-top	Wfr	2
Fractal width-down	Wf	0.1
Fractal length	Lfr	2.8
Shorting plate width	Ws	1.45
Shorting plate length	Ls	0.5
EBG unit cell width	P	3.6
Gap between two EBG neighboring cells	G	0.4

Table 11. The final antenna design with EBG structure dimensions.

The effects changing the EBG pad dimensions on the S_{11} spectrum is depicted in **Figure 28**. As can be observed, the best bandwidth enhancement is found when $P=3.6$ mm and $g=0.4$ mm.

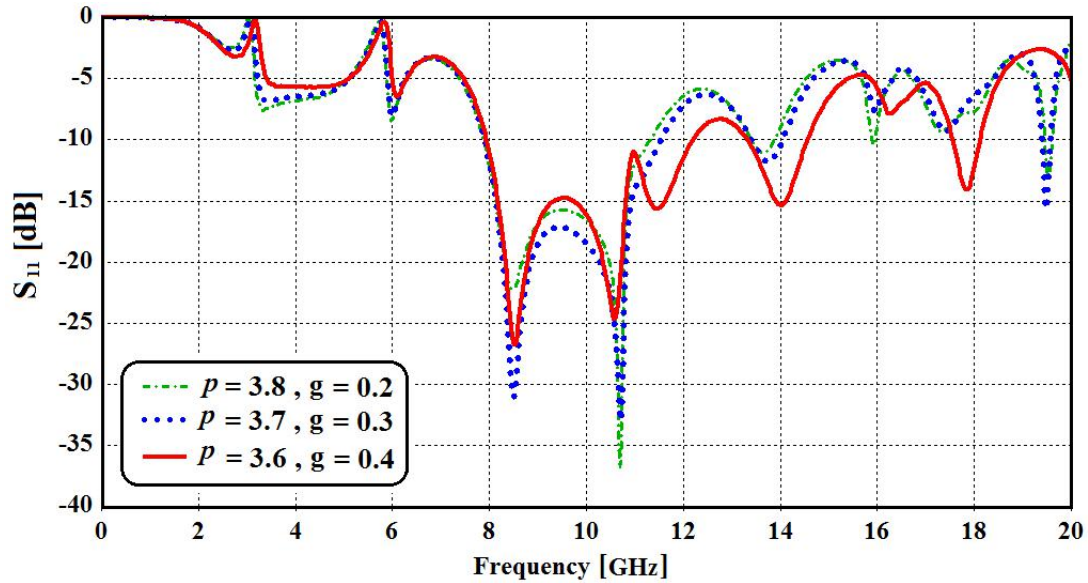


Figure 28; Effects of changing the EBG pad dimensions on the S_{11} spectra.

Effects of the Substrate Permittivity on the Proposed Antenna S_{11}

The consideration of the effect of substrate permittivity on S_{11} spectrum is conducted. From Figure 29, it can be seen the Roger RT 5880 with $\epsilon_r=2.2$ and $\tan\delta=0.00134$ provides a wider bandwidth than other substrates within the same thickness. Therefore, under this condition, the Roger RT 5880 is used for the proposed antenna.

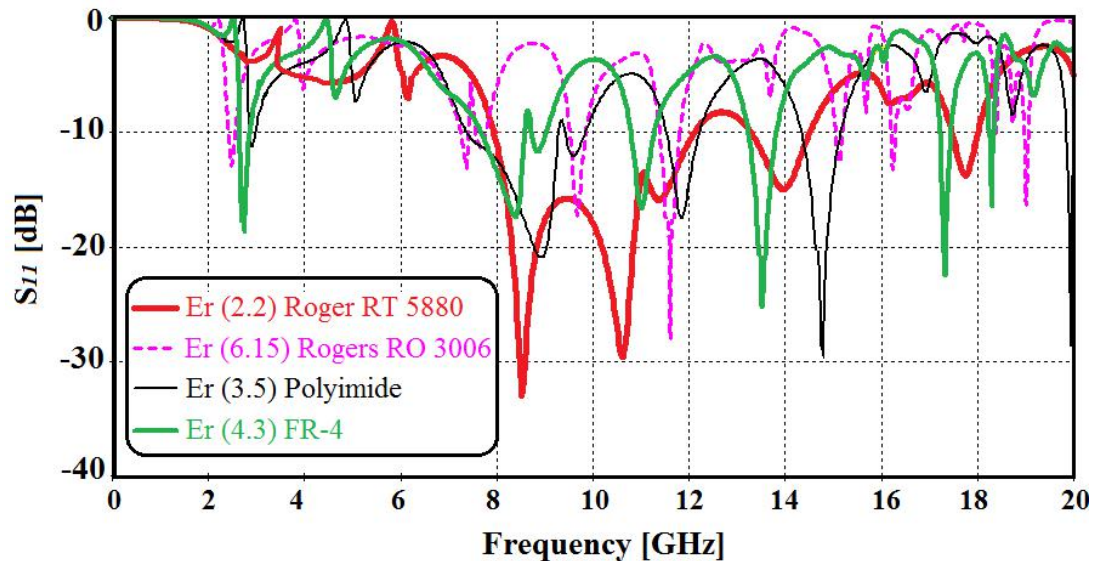


Figure 29; Effects of using different substrates on the S_{11} spectra.

Radiation Patterns of the Proposed Antenna

The objective of this section is to study the antenna radiation properties using CST MWS as shown in Figure 30. The radiation patterns of the antenna are illustrated in the E-plane (XZ-plane at $\theta=0$) and H-planes (YZ-plane at $\phi=90$). It is clearly seen that the radiation at 4 GHz is half wave dipole like whereas the antenna produces directional broadside pattern at 6 GHz. It can be noticed that the radiation pattern of the antenna design is toward the end-fire direction at 8 GHz to 10 GHz. This is accomplished by forcing the radiation to be directed along the end-fire by applying the flared reflectors. Nevertheless, the introduction of the EBG structure is to reduce the radiation leakage from the ground plane and providing more focusing toward the tangential radiation. However, the antenna shows broad side radiation at 14 GHz and the radiation goes back to be end fire at 17 GHz.

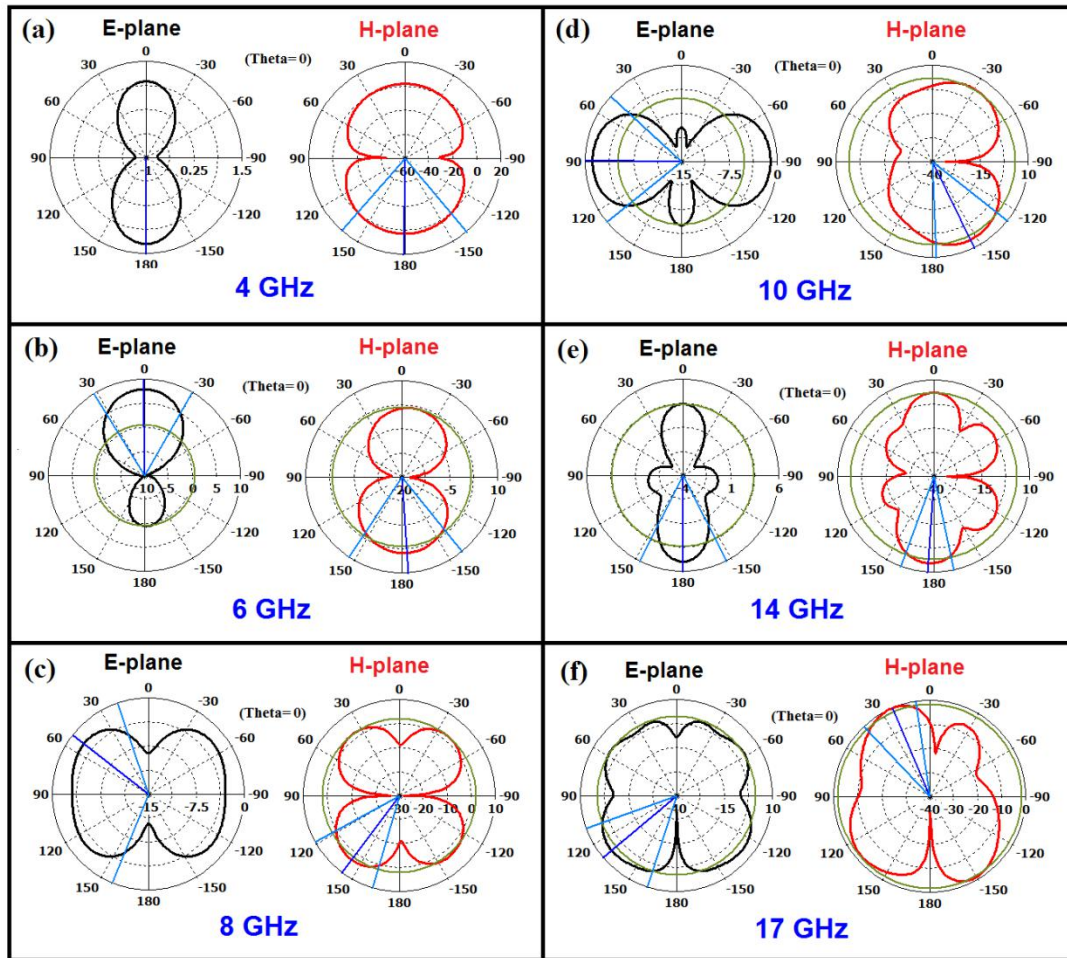


Figure 30; Simulated radiation patterns in polar plot at different frequencies: (a) 4 GHz, (b) 6 GHz, (c) 8 GHz, (d) 10 GHz, (e) 14 GHz and (f) 17 GHz.

3. Antenna Fabrication and Measurements

A wideband antenna is generally fabricated by photo-lithographic chemical etching method. Photo-lithographic method produces highly accurate etched patterns^[9]. The fabrication accuracy is very critical whereas any errors in the fabrication could shift the resonant frequency^[10]. Photo-lithographic method is a chemical etching process which removes the unwanted metal regions of the metallic layer^[8]. The fabricated prototype is depicted in **Figure 31**.

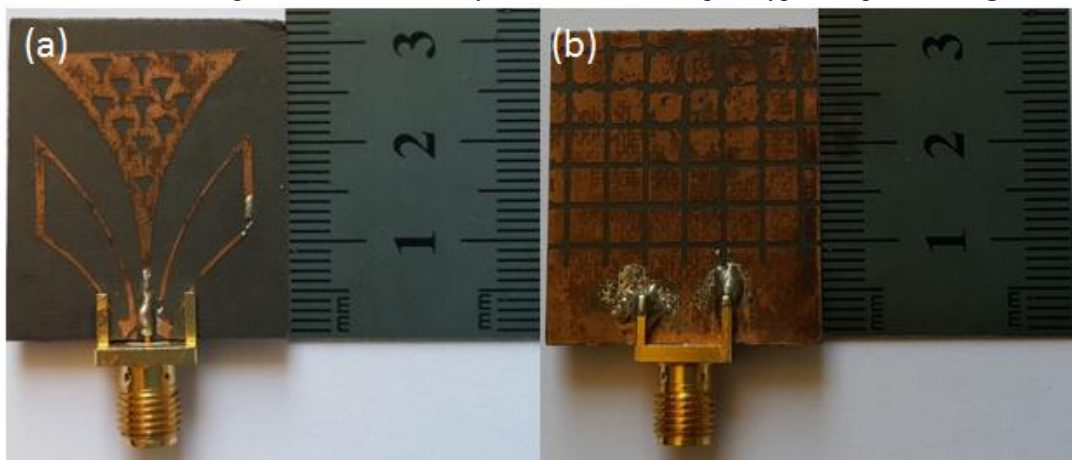


Figure 31; The fabricated antenna prototype: (a) Front view and (b) Back view.

The performance in terms of S_{11} of the implemented prototype is tested and measured then compared against the

numerical simulations as seen in **Figure 32(a)**. The HFSS simulation is invoked as a further validation for the obtained results from CST MWS before the antenna fabrication. A good agreement between the simulated and measured S_{11} spectra is achieved after invoking an Agilent N5230A Vector Network Analyzer (VNA). The measured S_{11} of the fabricated antenna shows a slight frequency shift with insignificant the S_{11} magnitude change. This may occur due to the unavoidable manufacturing tolerances. The far-field radiation patterns of the principal planes (E and H) are measured in a fully equipped anechoic chamber. The proposed antenna is placed on a positioner and aligned to a horn antenna with adjustable polarization. In Figures 32(b) and (c), the far-field radiation patterns of the fabricated prototype in the E- and H- planes are provided at 4 GHz with a gain of 5 dBi.

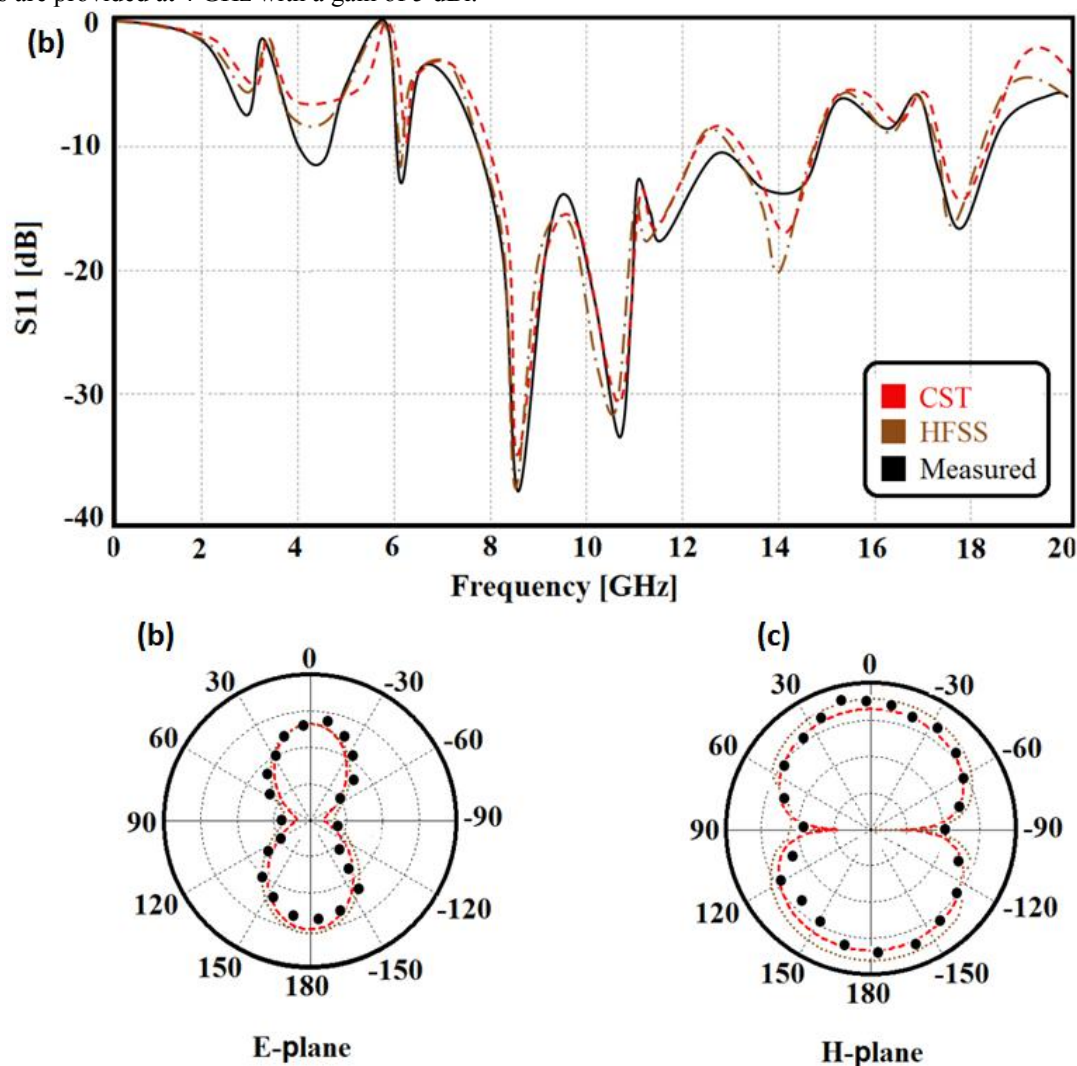


Figure 32; Comparison between measured and simulated results; (a) S_{11} spectra, far-field radiation patterns at 4 GHz in (b) E-plane and (c) H-plane.

4. Conclusion

In this paper, an intensive systematic study based on a parametric numerical simulation supported by both analytical derivation and measurements to design a lotus shaped microstrip antenna for wideband applications. The proposed antenna is constructed from a microstrip patch of lotus geometry defected with slots. The patch structure is fed with a novel flared CPW; where, the ground plane on the same substrate surface of the patch. The antenna ground plane is based on a partial defected EBG pads. The proposed antenna performance is tested numerically using CSTMWS and HFSS, then, compared against measurements for validation. It is found that the defected ground plane has a significant

effect on the antenna bandwidth with excellent gain enhancements at different frequencies. This observation is due to the ability of the EBG defects on suppressing the surface waves on the substrate. On top of that, the flared ground plane edges of the CPW structure provides a wide range of matching impedance that matches the antenna bandwidth over a wide range of frequencies. Therefore, the antenna bandwidth increased from 7.8GHz up to 15GHz and a matched frequency mode, $|S_{11}| < -10\text{dB}$, at 4 with 5dBi boresight gain.

References

1. Elwi TA. Potential Electromagnetic Researches based Artificial Material Structures for Advanced Photonics Devices. 2015 The 3rd Scientific Conference of ILPS 2015; 11.
2. Ibrahim OA, Elwi TA, Islam NE. A miniaturized microstrip antenna based on sinusoidal patch geometry for implantable biomedical applications. 6th Global Conference on Power Control and Optimization, AIP Conference Proceedings 2012; 1499(1): 254.
3. Elwi TA, Al-Rizzo HM, Y. Al-Naiemy Y, and H. R. Khaleel. Miniaturized microstrip antenna array with ultra mutual coupling reduction for wearable MIMO systems. 2011 IEEE International Symposium on Antennas and Propagation 2011; 7.
4. Elwi TA. A Miniaturized Folded Antenna Array for MIMO Applications. Wireless Personal Communications, DOI 10.1007/s11277-017-4950-4 2017; 9: 1-13.
5. Imran AI, Elwi TA. A cylindrical wideband slotted patch antenna loaded with frequency selective surface for MRI applications. Engineering Science and Technology, an International Journal 2017; 20(3): 990–996.
6. Elwi TA. Electromagnetic band gap structures based an ultra wideband microstrip antenna. Microwave and Optical Letters. February 2017; 59(4): 827-834.
7. Azeez AR, Elwi TA, AL-Hussain ZAA. Design and analysis of a novel concentric rings based crossed lines single negative metamaterial structure. Engineering Science and Technology. an International Journal 2016; 20(3): 1140–1146.
8. Azeez AR, Elwi TA, AL-Hussain ZAA. A numerical study of the antipodal vivaldi antenna design for ultra wideband applications. SAUSSUREA Multidisciplinary International Peer Reviewed Journal 2016; 6(5): 366-370.
9. Elwi TA, Imran AI, Alnaiemy Y. A miniaturized lotus shaped microstrip antenna loaded with EBG structures for high gain-bandwidth product applications. Progress In Electromagnetics Research C 2015; 60: 157-167.
10. Elwi TA, Hamed MM, Abbas Z, *et al.* On the performance of the 2D planar metamaterial structure. International Journal of Electronics and Communications 2014;68(9): 846–850.
11. Elwi TA, Al-Frieh S, Al-Bawi M, *et al.* No frequency reuse: wearable steerable MIMO microstrip antenna array for wearable ad hoc applications. British Journal of Applied Science & Technology 2014; 4(17): 2477-2488.
12. Elwi TA, Noori M, Al-Naiemy Y, *et al.* Conformal antenna array for MIMO applications. Journal of Electromagnetic Analysis and Applications 2014; 6: 43-50.
13. Ibrahim OA, Elwi TA, Islam NE. Gain enhancement of microstrip antennas using UC-PBG layer. Canadian Journal on Electrical and Electronics Engineering 2012; 3(9): 480-483.
14. Elwi TA. A further investigation on the performance of the broadside coupled rectangular split ring resonators. Progress In Electromagnetics Research Letters 2012;34: 1-8.
15. Elwi TA, Al-Rizzo HM, Bouaynaya N, *et al.* Theory of gain enhancement of UC–PBG antenna structures without invoking Maxwell’s equations: an array signal processing approach. Progress In Electromagnetics Research B 2011; 34: 15-30.
16. Elwi TA, Al-Rizzo HM. Fresnel lenses based on nano shell-silver coated silica array for solar cells applications. Progress In Electromagnetics Research B 2011;32: 263-282.
17. Elwi TA, Al-Rizzo HM, Rucker DG, *et al.* Effects of twisting and bending on the performance of a miniaturized truncated sinusoidal printed circuit antenna for wearable biomedical telemetry devices. AEU - International Journal of Electronics and Communications 2010;13(1): 1-12.
18. Elwi TA, Al-Rizzo HM, Rucker DG, *et al.* Numerical simulation of a UC–PBG lens for gain enhancement of microstrip antennas. International Journal of RF and Microwave Computer-Aided Engineering 2009; 19(6): 676–684.
19. Rahmat-Sami Y, Yang F, Kishk A. Low-profile patchfed surface wave antenna with a monopole-like radiation pattern. Microwaves, Antennas & Propagation, IET 2007; 1(1): 261 – 266.
20. Shaozhen Z, Langley R. Dual-band wearable textile antenna on an EBG substrate. IEEE Trans. on Antennas and Propagation 2009; 57(4): 926 – 935.
21. Lee H, Choi W. Effect of partial ground plane removal on the radiation characteristics of a microstrip antenna. Wireless Engineering and Technology 2013; 4(1): 5-12.
22. Lech R, Marynowski W, Kusiek A. Finite ground CPW fed UWB antenna over the metallic cylindrical surfaces. Progress In Electromagnetics Research 2013; 140: 545-562.
23. He SH, Shan W, Fan C, *et al.* An improved vivaldi antenna for vehicular wireless communication systems. IEEE

Antennas and Wireless Propagation Letters 2014; 13: 1505–1508.

24. Mohamad S, Cahill R, Fusco V. Performance of archimedean spiral antenna backed by FSS reflector. *Electronics letters*, IEEE 2015; 51(1): 14 – 16.
25. Kurra L, Abegaonkar MP, Basu A, *et al.* FSS properties of a uni-planar EBG and its application in directivity enhancement of a microstrip antenna. *IEEE Antennas and Wireless Propagation Letters* 2016; 99: 1- 5.
26. Garg R, Bhartia P, Bhal I, *et al.* *Microstrip antenna design handbook*, 1st edition. Artech House Inc. 2001.
27. Balanis CA. *Antenna theory: analysis & design*. 3th edition, John Willey & Sons, Inc., Boston 2005 ; 24 (6) :28-29.
28. Nihad ID, Olaimat MM. Improved formulae for the resonant frequencies of triangular microstrip patch antennas. *International Journal of Electronics* , Taylor & Francis 2011; 98(3): 407–424.
29. Zhao W. *Novel metamaterials and their applications in subwavelength waveguides, imaging and modulation*. Ph.D. Book, University of Rochester at Kate Gleason College of Engineering, New york 2014.
30. Luukkonen O, Simovski C, Granet G, *et al.* Simple and accurate analytical model of planar grids and high-impedance surfaces comprising metal strips or patches. *IEEE Trans. On Antennas and Propagation* 2008; 56(6): 1624 – 1632.
31. Yang F, Rahmat-Samii Y. *Electromagnetic band gap structures in antenna engineering*. 1st edition, Cambridge University Press 2009.
32. Wadell BC. *Transmission line design handbook*. 1st edition, Artech House Inc. 1991.
33. Bus BA, Arias-Vasquez A, Franke B, *et al.* Generalized retrieval method for metamaterial constitutive parameters based on a physically driven homogenization approach. e-print: arXiv: 1303.5807 2013 ; 87 (23) :291-295.
34. Hossain MI, Faruque MRI, Islam MT, *et al.* A new wide-band double-negative metamaterial for C- and Sband applications. *Materials* 2014;8: 57-71.
35. Mitzner K. *Complete PCB design using or CAD capture and layout*. 1st edition, Newnes, Inc. 2007.
36. Ali J, Yahya R, Abdullah N, *et al.* Ultra-wideband monostatic antenna for behind the wall detection. *International Journal of Electrical and Computer Engineering* 2017; 7(6).